Neurobiology of Disease 201 (2024) 106670

Contents lists available at ScienceDirect

Neurobiology of Disease

journal homepage: www.elsevier.com/locate/ynbdi

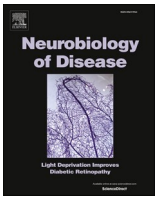

Astrocyte TrkB promotes brain injury and edema formation in ischemic stroke

Emanuela Colombo [a], Marco Bacigaluppi [b,c], Michela Bartoccetti [a], Daniela Triolo [a], Claudia Bassani [a], Andrea Bergamaschi [b], Hélène C. Descamps [b], Giorgia Serena Gullotta [b], Maria Henley [d], Marco Piccoli [e], Luigi Anastasia [c,e], David Pitt [d], Jia Newcombe [f], Gianvito Martino [b,c], Cinthia Farina [a,*]

[a] Immunobiology of Neurological Disorders Unit, Institute of Experimental Neurology (INSpe), IRCCS San Raffaele Scientific Institute, Milan, Italy
[b] Neuroimmunology Unit, Institute of Experimental Neurology, IRCCS San Raffaele Scientific Institute, Milan, Italy
[c] University Vita-Salute San Raffaele, Milan, Italy
[d] Department of Neurology, Yale School of Medicine, New Haven, CT 06510, USA
[e] Institute for Molecular and Translational Cardiology (IMTC), IRCCS Policlinico San Donato, Milan, Italy
[f] NeuroResource, Department of Neuroinflammation, UCL Queen Square Institute of Neurology, London, UK

ARTICLE INFO

Keywords:
AQP4
Astrocyte
Stroke
TrkB

ABSTRACT

Following ischemic stroke astrocytes undergo rapid molecular and functional changes that may accentuate tissue damage. In this study we identified the neurotrophin receptor TrkB in astrocytes as a key promoter of acute CNS injury in ischemic stroke. In fact, TrkB protein was strongly upregulated in astrocytes after human and experimental stroke, and transgenic mice lacking astrocyte TrkB displayed significantly smaller lesion volume, lower brain atrophy and better motor performance than control animals after transient middle cerebral artery occlusion. Neuropathological studies evidenced that edema directly correlated with astrogliosis and was limited in transgenic mice. Importantly, adaptive levels of the water channel AQP4 was astrocyte TrkB-dependent as AQP4 upregulation after stroke did not occur in mice lacking astrocyte TrkB. *In vitro* experiments with wild-type and/or TrkB-deficient astrocytes highlighted TrkB-dependent upregulation of AQP4 *via* activation of HIF1-alpha under hypoxia. Collectively, our observations indicate that TrkB signaling in astrocytes contributes to the development of edema and worsens cerebral ischemia.

1. Introduction

Ischemic stroke is a leading cause of disability and death in adulthood worldwide (Campbell and Khatri, 2020). It consists of an acute episode of injury caused by cerebral arterial occlusion leading to irreversible cell death in the area where blood flow is heavily impaired (ischemic core) and cell dysfunction in the surrounding peri-ischemic regions (penumbra), characterized by hypoxia and low levels of nutrients (Campbell and Khatri, 2020). Currently approved therapies for ischemic stroke target blood vessel occlusion to achieve tissue reperfusion but improve clinical condition and central nervous system (CNS) function if administered within a few hours after the onset of the ischemic event (Chamorro et al., 2021). As neural tissue in the ischemic core becomes irreversibly damaged, novel therapeutic approaches aiming to limit infarct size and maintain function in neighboring areas represent an unmet clinical need (Yang and Liu, 2021).

Following ischemia, astrocytes in peri-ischemic areas undergo phenotypical and functional changes that result in enhanced glial fibrillary acidic protein (GFAP) expression, hypertrophy and proliferation (Shen et al., 2021). They may release mediators that enhance brain

Abbreviations: 2ME2, 2-methoxyestradiol; AQP4, Aquaporin 4; BBB, blood brain barrier; BrdU, 5-bromo-2-deoxyuridine; BSA, bovine serum albumin; CNS, central nervous system; DAPI, 4,6-diamidino-2-phenylindole; FBS, fetal bovine serum; GFAP, glial fibrillary acidic protein; GLAST, glutamate aspartate transporter; GLT1, glial glutamate transporter 1; MCAO, Middle cerebral artery occlusion; MRI, Magnetic Resonance Imaging; PBS, phosphate-buffered saline; PFA, paraformaldehyde; TBS, Tris buffered saline; TrkB, tropomyosin receptor kinase B..

* Corresponding author at: Institute of Experimental Neurology (INSpe) and Division of Neuroscience, IRCCS San Raffaele Scientific Institute, Via Olgettina, 58, 20132 Milan, Italy.
E-mail address: farina.cinthia@hsr.it (C. Farina).

https://doi.org/10.1016/j.nbd.2024.106670
Received 23 July 2024; Received in revised form 13 September 2024; Accepted 15 September 2024
Available online 18 September 2024

edema and neurotoxicity, and inhibit axonal regeneration (Lo et al., 2005; Dvoriantchikova et al., 2009; Overman et al., 2012). On the other hand, astrocyte scar formation around the infarct core may restrict lesion volume and support neuronal plasticity and survival (Li et al., 2008; Cekanaviciute et al., 2014; Shen et al., 2021). *In vivo* studies of CNS inflammatory diseases using cell type-specific transgenic mice provided key information about how perturbations in single signaling pathways may affect disease outcome (Colombo and Farina, 2016). However, efforts to translate this knowledge to widespread, acute CNS injury following ischemic stroke have been limited. Here, we investigated the contribution of astrocyte tropomyosin receptor kinase (Trk) B to brain ischemia using the middle cerebral artery occlusion (MCAO) experimental model and human stroke specimens, and combining *in vivo* with *ex vivo* and *in vitro* approaches. Collectively, our observations highlight TrkB signaling in astrocytes as a key checkpoint supporting cerebral ischemia pathogenesis *via* regulation of edema.

2. Materials and methods

2.1. Mice

In vivo experiments were performed on 8–12-week-old male C57BL/6 wild type mice (purchased at Envigo), GFAPcre:TrkBflox/flox (GFAPTrkB KO) conditional mutant mice and control TrkBflox/flox (TrkB WT) littermates. GFAPTrkB KO mice and control TrkB WT littermates were bred at IRCCS San Raffaele Scientific Institute (Colombo et al., 2012; Colombo et al., 2021). All mice were bred in the same animal house, maintained under specific pathogen-free conditions and housed 2–5 per cage in a 12-h light: dark cycle with *ad libitum* access to food and water.

2.2. Middle cerebral artery occlusion (MCAO) model generation and analysis

Animals were anesthetized with 1–1.5 % isoflurane (Merial) in 30 % O2 (remainder N2O). Rectal temperature was maintained between 36.5 and 37.0 °C using a feedback-controlled heating system (Harvard Instruments). Considering the left–right asymmetry in the rodent brain and its impact on neurological and pathological outcomes after ischemia (Ma et al., 2020), left middle cerebral artery occlusion was induced for 45 min with a silicon-coated (Xantopren, Bayer Dental) 8–0 nylon filament (Ethilon, Ethicon) as previously described (Gullotta et al., 2023). To correct fluid loss during the surgical intervention, 0.5 ml of 0.9 % NaCl was intraperitoneally injected in each animal every day for the first three days after MCAO.

For the measurement of total ischemic volume in live animals, mice were anesthetized and subjected to brain magnetic resonance imaging (MRI) at day 7 post-ischemia (p.i.) in a 7 Tesla small-bore Magnetic Resonance scanner for small animals (Bruker BioSpec® 70/30). A channel rat heart coil was employed for acquiring Turbo Spin Echo T2 images (TR2137, TE12, Effective TE36, Voxel 98x98x700μm). Volumes were measured on coronal T2 images by OsiriX Imaging Software and then calculated as described in (Bacigaluppi et al., 2016). Data were expressed as percentage of contralateral hemisphere.

Asymmetry of forelimb movements was assessed using the cylinder test (Balkaya et al., 2013). Mice were placed in a plexiglass cylinder and their spontaneous activity to rear up on hind limbs and explore the vertical surface with forelimbs was observed. The number of times mice used their ipsilateral, contralateral or both forepaws to touch the cylinder wall was recorded. Recording stopped after 10 min or when the total number of contacts reached 20. The asymmetric score was calculated as (the number of ipsilateral paw touches − number of contralateral paw touches)/total number of touches. All tests were performed by trained investigators blinded to the genotype during the light phase of the circadian cycle beginning 4 h after lights on.

To measure astrocyte proliferation *in vivo,* 50 mg/kg of 5-bromo-2-deoxyuridine (BrdU, Sigma-Aldrich) was intraperitoneally administered at day 0, 3 or 10 post-ischemia, two injections a day till sacrifice three days later. At the end of the experiment, mice were perfused with 4 % paraformaldehyde (PFA) and brains were extracted and used for immunohistochemical/immunofluorescence studies. Age-matched male mice with no ischemia were sacrificed and used for comparative analyses.

2.3. Histological analyses of infarct size, edema and atrophy

Mouse brains were removed from 4 % PFA-perfused mice, postfixed overnight, cryoprotected in sucrose, embedded in optimal cutting temperature embedding medium for cryostat sectioning (Bio-Optica) and rapidly frozen in isopentane precooled in liquid nitrogen. Frozen brains were cut into 20 μm-thick coronal sections at 600 μm interval from 2 mm rostral to 4 mm caudal to the Bregma. For infarct size determination one series of sections per mouse was stained with cresyl violet (Sigma-Aldrich), digitalized and analyzed with ImageJ (download at: http://rsbweb.nih.gov/ij/) and QuPath (download at: https://qupath.github.io/) softwares. Infarct volumes were determined by the 'indirect method' (Lin et al., 1993). Briefly, for each section the edema-adjusted infarct area was calculated by subtracting the non-infarcted area in ipsilateral hemisphere from the contralateral hemisphere area and multiplied by the 600 μm interval so to generate a series of infarct volume values which were summed up and expressed as percentage of total contralateral volume. Edema was measured at 24 h p.i. and calculated by subtracting the ischemic hemisphere volume from the contralateral hemisphere volume and expressed as percentage of contralateral volume. The same analysis was performed at 34 days p.i. to evaluate atrophy index.

2.4. Human brain samples

Post-mortem brain samples were obtained from 3 subjects with acute cerebral infarcts (infarct to postmortem intervals between 25 and 37 h; 1 female and 2 males, mean age 76 ± 12.5), 3 subjects with chronic cerebral infarcts (infarct to postmortem intervals between 2 and 9 years; 1 female and 2 males, mean age 69 ± 9.8) and 4 control donors (2 females and 2 males, mean age 76.3 ± 2.9). Tissues from subjects with acute ischemia were obtained at autopsy according to the Review Board-approved protocol at Department of Neurology, Yale School of Medicine, USA, fixed in 10 to 20 % formalin for 2 to 4 weeks, then embedded in paraffin. Preliminary histological examination of large brain sections was instrumental for selection of tissue slices spanning from infarcted area to morphologically normal regions. As far as regards samples from subjects with chronic cerebral infarcts, gliotic white matter tissues immediately close to the infarct and control samples were provided by the NeuroResource tissue bank (UCL Queen Square Institute of Neurology, London, UK), donated with informed consent using documentation approved by the NHS NRES Ethics Committee London–Central, UK, and stored as snap-frozen tissue blocks under a Research Sector Licence from the UK Human Tissue Authority (HTA). All procedures involving analyses of human specimens were approved by the ethical committee at IRCCS San Raffaele Scientific Institute and performed in accordance with the ethical standards as laid down in the 1964 Declaration of Helsinki and its later amendments or comparable ethical standards. Seven or twelve μm-thick sections were prepared from human paraffin embedded blocks or snap-frozen brain tissue blocks respectively.

2.5. Tissue protein immunohistochemistry and immunofluorescence

For immunohistochemical stains, endogenous peroxidase was neutralized with 5 % H_2O_2 in methanol and unspecific binding was blocked in a phosphate-buffered saline (PBS) solution containing 1 % Bovine Serum Albumine (BSA) (Merck) and 5 % fetal bovine serum

(FBS) (Euroclone). PFA-fixed sections were then stained with primary antibodies. Bound primary antibodies were visualized with appropriate species-specific HRP-conjugated secondary antibodies or avidin–biotin–peroxidase complex and with 3,3′-diamonobenzidine (DAB; Agilent) as chromogen. Counterstaining with hematoxylin was then performed.

For immunofluorescence stains of frozen human or mouse tissues, after blocking PFA-fixed sections were first incubated with primary antibodies and then with appropriate species-specific Alexa Fluor 488/594/647-conjugated secondary antibodies (Thermo Fisher Scientific). Slides were counterstained with 4′,6-diamidino-2-phenylindole (DAPI, Sigma-Aldrich) and mounted with fluorescent mounting medium (Agilent). For BrdU detection, DNA was depurinated to make epitopes accessible to antibodies by incubating slides in 2 N HCl for 30 min. Slides were then rinsed in borate buffer (0.1 M, pH 8.5) for 10 min at room temperature. Paraffin embedded human sections were deparaffinized, subjected to antigen retrieval using citrate buffer pH 6.0 for 25 min, then permeabilized in a Tris buffered saline (TBS) solution containing 0.5 % Triton X-100. After washing in 1XTBS and 0.01 % Tween 20, sections were quenched in 0.3 % H2O2 in TBS for 1 h then blocked using 10 % Normal Goat Serum and 10 % FcR inhibitor (Invitrogen). After incubation with primary and species-specific secondary antibodies, slides were stained with Sudan black (MP Biomedicals) to reduce autofluorescence and counterstained with Hoechst 33342 (Life Technologies), and covered with 50 % glycerol in water.

The following primary antibodies were used: rabbit anti-GFAP (1:200, Agilent); rat anti-GFAP (1:200; Thermo Fisher Scientific), mouse anti-GFAP (1:200, BD Biosciences), chicken anti-GFAP (1:400, Biolegend), rat anti-BrdU (1:100, Abcam), rabbit anti-Iba1 (1:800, FUJIFILM Wako Chemicals, Germany); mouse anti-TrkB (1:100, R&D, Canada), goat anti-TrkB (1:200, R&D), rabbit anti-TrkB (1:1000, Genetex), rabbit anti-TrkB.T1 (1:50, Absolute antibody), rabbit anti-AQP4 (1:200, Millipore), guinea pig anti-AQP4 (1:200, Synaptic Systems), rabbit anti-HIF-1α (1:100, Cell Signaling), rabbit anti-AQP4 (1:250) rabbit anti-GLAST (1:200, Abcam), guinea pig anti-GLT1 (1:100, Millipore), biotinylated goat anti-mouse IgG (1:500, Vector Laboratories). The following secondary antibodies were used: HRP labelled Polymer anti-rabbit/goat/guinea pig (Jackson Laboratories), Alexa Fluor 488/594 donkey anti-rabbit/mouse IgG (H + L) (1:1000, Thermo Fisher Scientific), Alexa Fluor 488 goat anti-rabbit IgG (H + L) (1:1000, Thermo Fisher Scientific), Alexa Fluor 488/594/647 donkey anti-rat IgG (H + L) (1:1000, Thermo Fisher Scientific), Alexa Fluor 546 goat anti-chicken IgY (H + L) (1:1000, Thermo Fisher Scientific), Alexa Fluor 647 goat anti-guinea pig (H + L) (1:1000, Thermo Fisher Scientific). As negative controls, mouse IgG1 (Sigma-Aldrich), rat IgG1 (Biolegend) or rabbit immunoglobulins (Ig) (Thermo Fisher Scientific) were used at the same concentration of the primary antibodies. Immunohistochemistry images were acquired with a Leica DM5500B light microscope or Aperio AT2 digital scanner (Leica Biosystems). Fluorescence images were captured with a Leica TCS SP5 confocal laser-scanning microscope equipped with 40× and 63× oil objectives or with a Leica Microsystems Thunder imager at 20× and 40× magnification. Acquisition settings were set on negative controls and single stacks were acquired by LASAF, LASX or Leica Thunder softwares. ImageJ and QuPath softwares were used for blinded image analysis. For the measurement of fluorescence signals, eight to ten fields were acquired for each sample of human or rodent tissues. Then, a threshold specific for each experiment was set on negative control and immunohistochemical/fluorescence signal was measured above the threshold and calculated as percentage of positively stained area on the entire measured area.

2.6. Generation and in vitro stimulation of primary astrocytes

Primary astrocytes were prepared from brains of male or female GFAPTrkB KO and control (TrkB WT) littermates according to published protocols (Colombo et al., 2021). Briefly, primary mixed glial cultures were established from the forebrains of 1 day old pups, mechanically dissociated and digested with 0.25 % trypsin solution. Mixed cultures were maintained in Dulbecco's modified eagle medium-high glucose medium containing 1 % antibiotics (Pen/Strep solution), 200 mM L-Glutamine, 100 mM Sodium Pyruvate (all from Gibco) and 10 % FBS (Euroclone, Italy). 10-day-old primary cultures were vigorously shaken to discard microglia and oligodendrocytes. The remaining adherent cells were detached and, following an adhesion step, non-adherent cells were reseeded on poly-D-lysine (Sigma-Aldrich) coated flasks in complete medium. Purity of astrocyte cultures was >95 % according to GFAP immunofluorescence.

For hypoxia *vs.* normoxia assays cells were plated on glass coverslips and cultured in a 5 % CO_2, 20 % O_2 HERAcell incubator (ThermoFisher Scientific) (normoxic conditions) or in a 5 % CO_2, 1 % O_2 hypoxic workstation (SCI-tive, Baker Ruskinn) (hypoxic conditions). To inhibit hypoxia-inducible factor 1-alpha (HIF-1α) astrocytes were treated with 50 μM 2-methoxyestradiol (2ME2) or vehicle (0.3 % DMSO) for 2 h under normoxia, then further incubated under normal or hypoxic conditions in fresh medium. Cells were then processed for immunofluorescence and stained with appropriate primary antibodies. Technical triplicates were used for each condition and at least 100 cells per replicate were analyzed.

2.7. Immunocytochemistry

Primary astrocytes were fixed in 4 % PFA, permeabilized with 0.2 % Triton X-100 (Merck) or 0.1 % Saponin, blocked in PBS + 1 % BSA (Merck) + 5 % FBS and stained with primary antibodies. Then, cells were incubated with appropriate species-specific Alexa Fluor 488-conjugated secondary antibodies (Thermo Fisher Scientific), counterstained with 4,6-diamidino-2-phenylindole (DAPI, Sigma-Aldrich) and mounted with fluorescent mounting medium (Agilent). The following primary antibodies were used: rabbit anti-TrkB (1:1000, Genetex), rabbit anti-AQP4 (1:200, Millipore), rabbit anti-HIF-1α (1:100, Cell Signaling). Fluorescence images were captured at fluorescence microscope (Olympus BX51), LASX softwares was used for image acquisition and ImageJ (download at: http://rsbweb.nih.gov/ij/) software was used for image analysis. To quantify nuclear HIF-1α, DAPI images were converted to 8-bit, ROIs were generated to select (DAPI positive) nuclei and applied to the corresponding HIF-1α images. Fluorescence thresholds were fixed on the unstimulated condition and the fraction of positive nuclei was assessed. Similarly, the fraction of highly fluorescent astrocytes above the threshold was used to quantify cellular TrkB and Aquaporin (AQP) 4 expression under distinct conditions.

2.8. Statistical analysis

Data in figures are presented as mean ± standard error of the mean (SEM) or standard deviation (SD) as indicated in figure legends. The exact number of mice, samples, or performed independent experiments is reported in figure legends. Normality of the distribution was assessed by Kolmogorov-Smirnov statistics. ANOVA/ *t*-test (in case of normal distribution) or non-parametric Mann-Whitney *U* Test (in case of non-normal distribution) were performed to compare means. All *p*-values were two-sided and subjected to a significance level of 0.05. In figures, asterisks denote statistical significance as * $p < 0.05$; ** $p < 0.01$; *** $p < 0.001$. Statistical analyses were performed in Excel or GraphPad Prism.

3. Results

3.1. Astrocyte TrkB is upregulated in human and experimental brain ischemia

Confocal imaging of immunofluorescent stains revealed strong upregulation of TrkB protein on human astrocytes located in peri-infarct

specimens compared to control tissues (Fig. 1A). Signal quantification in distinct areas of control or peri-ischemic regions underlined the direct and significant correlation between TrkB and GFAP levels (Fig. 1B).

To study astrocytosis in experimental stroke, C57BL/6 adult mice were subjected to 45 min of transient MCAO, administered with BrdU at day 0, 3 or 10 post-ischemia (p.i.) for three days and then sacrificed (day 3, 6 or 13 p.i.). Confocal imaging analysis of tissues revealed that, compared to CNS samples of healthy control mice, ischemic hemispheres of MCAO mice showed significant induction of astrocyte proliferation starting at day 3 p.i. (Fig. 1C-D) and rising GFAP expression along time (Fig. 1E-F). Notably, astrogliosis was associated with increasing TrkB protein levels in MCAO tissues (Fig. 1E,G).

3.2. TrkB deletion in glia cells restricts experimental stroke

To verify the contribution of astrocyte TrkB to acute CNS injury, we induced MCAO in double transgenic mice lacking TrkB in GFAP-positive cells (GFAPcre:TrkBflox/flox genotype, hereafter referred to as GFAPTrkB KO mice) and control wild type littermates (TrkBflox/flox genotype, hereafter referred to as TrkB WT mice) (Colombo et al., 2012; Colombo et al., 2021).

7 T-MRI imaging at day 7 p.i. showed significantly lower infarct volumes in GFAPTrkB KO mice compared to TrkB WT mice (Fig. 2A-B). Ischemic stroke strongly impaired motor coordination as measured by the cylinder test, so that TrkB WT MCAO mice showed clear preferential usage of the ipsilateral forelimb at day 7 p.i., a behavior from which they partly recovered along time (mean asymmetric score = 0.43 and 0.28 at day 7 and day 25 respectively). Notably, GFAPTrkB KO mice displayed little or no asymmetry of forelimb movements (mean asymmetric score < 0.02 at any time points) (Fig. 2C), demonstrating that astrocyte TrkB supports the dysfunction of motor coordination after stroke.

Histological evaluation of ischemic brains in the acute (day 1 p.i.) and chronic phases (day 34 p.i.) of the disease confirmed low infarct volumes at both time points (Fig. 2d-f) and significantly reduced brain atrophy in the chronic phase (Fig. 2G) for the transgenic animal group.

Compared to non-ischemic mice, both groups of infarcted animals displayed higher GFAP levels in the infarcted hemisphere at day 1 p.i. (Fig. 2H, J black dots), however, GFAP up-regulation was significantly lower in GFAPTrkB KO mice than in control littermates (Fig. 2H, J white dots). Astrocytosis further increased in the damaged hemisphere during the chronic phase after ischemic injury and became evident also in the contralateral hemisphere (Fig. 2I-J black dots). Even at the late time point (day 34 p.i.), astrocyte reactivity was lower in GFAPTrkB KO mice, indicating that astrocyte TrkB is an important contributor to scar

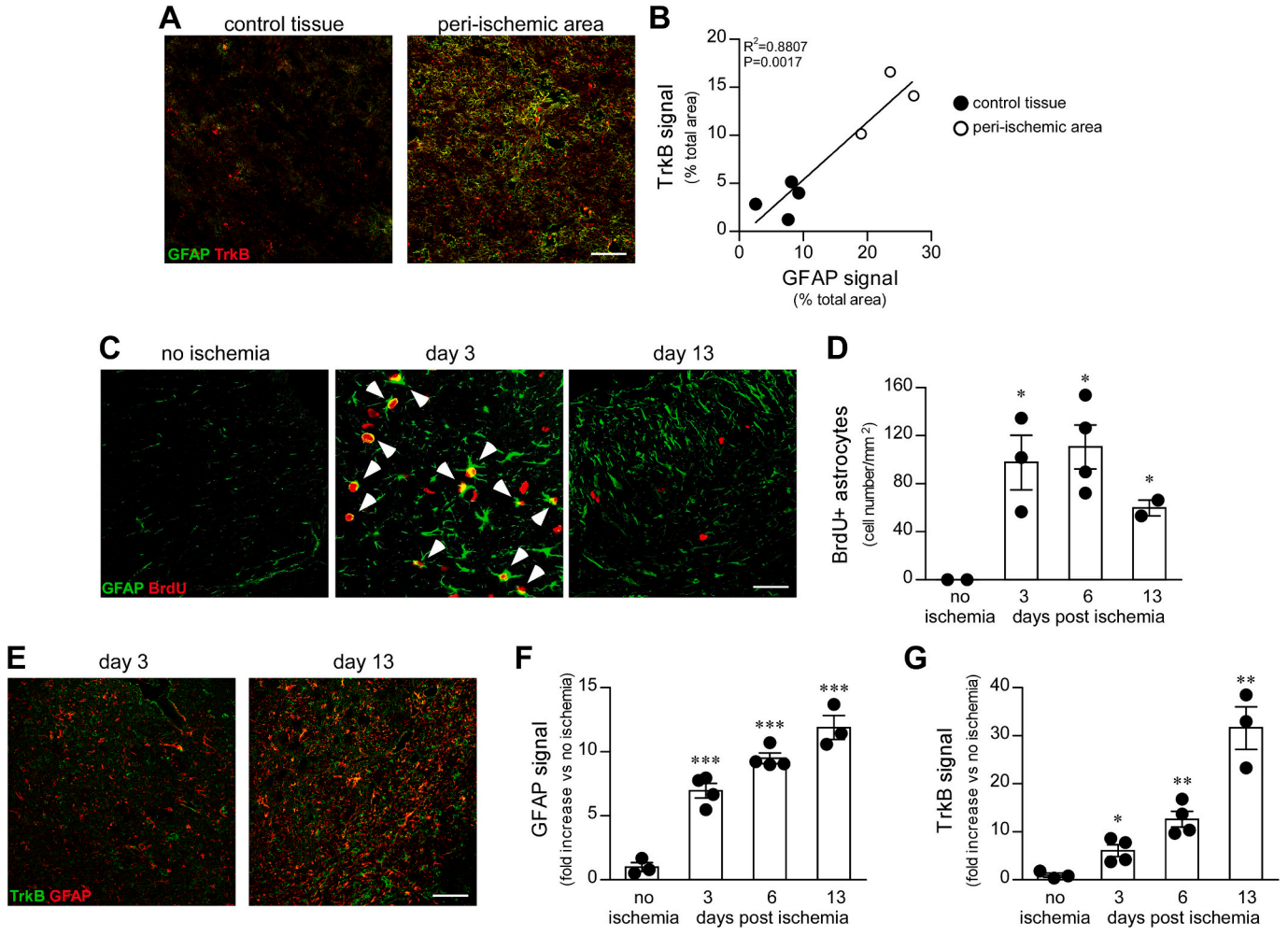

Fig. 1. Astrocyte TrkB is upregulated in human and experimental brain ischemia. (A) Representative immunofluorescence stains for GFAP (green) and TrkB (red) in human control (left panel) or peri-ischemic tissues (right panel). (B) Correlation between TrkB and GFAP expression in control ($n = 4$) and peri-ischemic tissues ($n = 3$). (C—D) Representative immunofluorescence stains for GFAP (green) and BrdU (red) in healthy brain samples and ischemic hemispheres at distinct time points after MCAO, and relative quantifications. White arrows in (C) highlight BrdU+ astrocytes. (E) Representative double immunofluorescence stains for GFAP (red) and TrkB (green) in ischemic tissues at distinct time points p.i., and signal quantifications compared to non-ischemic brain (F-G). Asterisks indicate statistical significance *versus* no ischemia. ***$P < 0.001$, **$P < 0.01$, *$P < 0.05$. In B, D, F, and G, each dot represents a single sample or animal; bars represent means of the values ± SEM. Scale bars 50 μm. (For interpretation of the references to colour in this figure legend, the reader is referred to the web version of this article.)

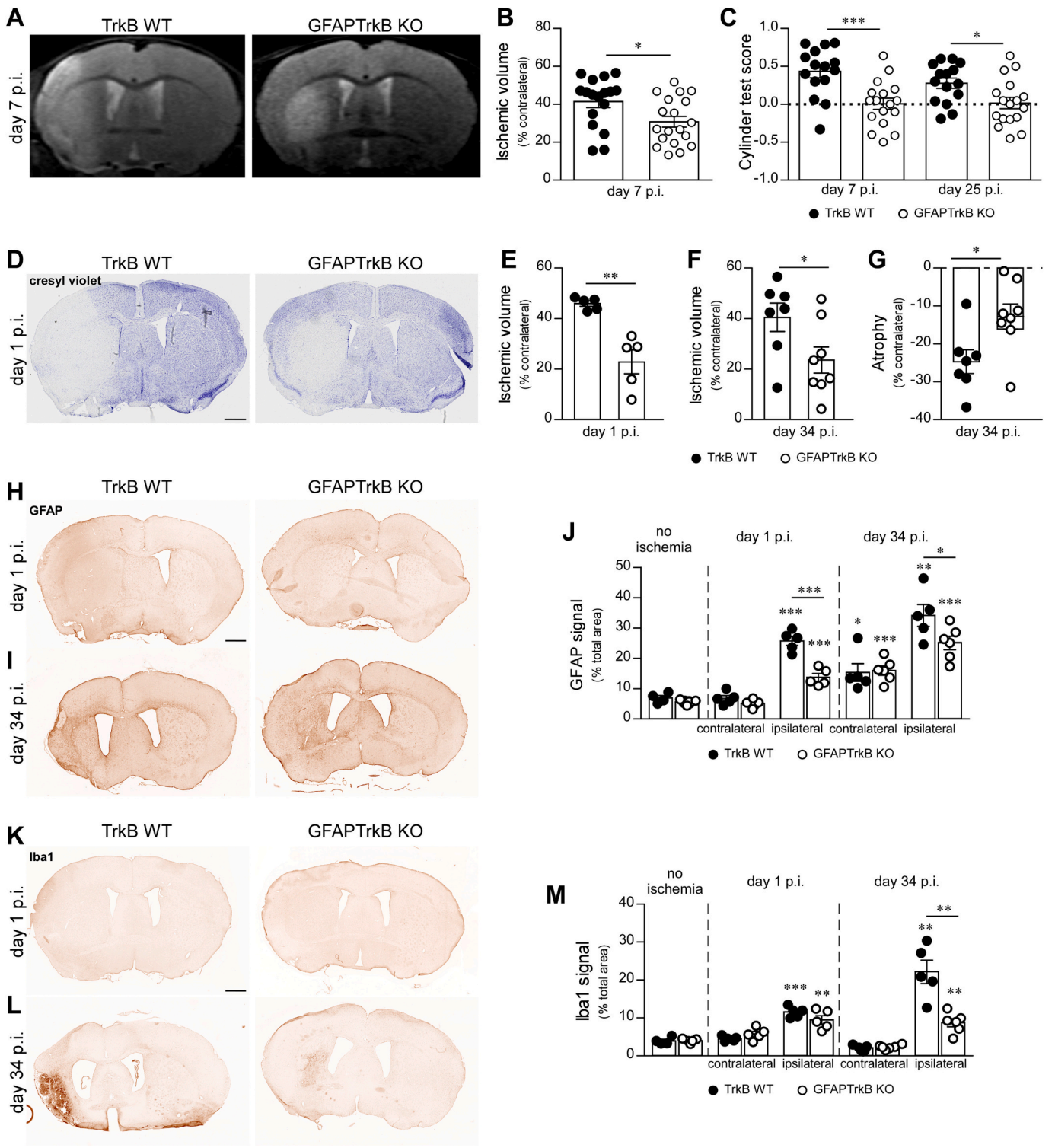

Fig. 2. TrkB deletion in glia cells restricts experimental ischemic stroke. (A-B) Representative T2-weighted brain MRI images of TrkB WT or GFAPTrkB KO mice at day 7 p.i. (A) and quantification of infarct volume as detected by MRI (B). (C) Motor performance of TrkBWT or GFAPTrkB KO animals at day 7 and 25 days p.i. (D) Representative ischemic brain sections stained with cresyl violet relative to TrkB WT and GFAPTrkB KO mice at day 1 p.i. (*E*-F) Quantification of ischemic volume in TrkB WT or GFAPTrkB KO mice at day 1 (E) or 34 (F) p.i. as assessed by cresyl violet stain. (G) Atrophy in ischemic hemispheres of TrkB WT or GFAPTrkB KO mice at day 34 p.i. as elaborated from cresyl violet stain. (H—I) Representative brain immunohistochemistry for GFAP in TrkBWT and GFAPTrkB KO mice during stroke. (J) Quantification of GFAP signal in the contralateral and ipsilateral hemispheres of non-ischemic animals and mice subjected to MCAO. (K-M) The same as in (H-J) for Iba1 stain. Asterisks indicate statistical significance *versus* no ischemia. Asterisks above bar indicate statistical significance between different genotypes. ***P < 0.001, **P < 0.01, *P < 0.05. In B—C data from animals derived from two independent experiments are reported. In B, C, E, F, G, J, M each dot represents a single animal; bars represent means of the values ± SEM. Scale bars 800 μm. (For interpretation of the references to colour in this figure legend, the reader is referred to the web version of this article.)

formation after stroke (Fig. 2I-J white dots). As detected by Iba1 stain, microglia activation in the infarcted hemisphere was quite modest at day 1 p.i. in both groups of animals (Fig. 2K, M), but very evident in the chronic phase (Fig. 2L-M). At this late stage the labeling pattern differed between genotypes and was approximately 60 % lower in GFAPTrkB KO mice (Fig. 2L-M).

Overall, these *in vivo* results indicate a pathogenic role for astrocyte TrkB in the evolution of experimental stroke.

3.3. Astrocyte TrkB does not modulate glutamate transporter levels

Glutamate-induced excitotoxicity is a major cause of neuronal death after ischemic stroke. As glutamate uptake is primarily achieved by astrocytes through the glutamate aspartate transporter (GLAST) and glial glutamate transporter 1 (GLT1) (Kaplan-Arabaci et al., 2022), we analyzed the expression of these transporters in brain tissues from TrkB WT and GFAPTrkB KO mice by immunohistochemistry. Compared to the healthy CNS, GLAST and GLT1 signals were higher in the ischemic but not in the contralateral hemispheres of wild type and GFAPTrkB KO mice at day 1 p.i. (Fig. 3A-B; *E*-F), while equally expressed in both hemispheres at day 34 p.i. (Fig. 3C-D; G-H). No difference emerged between wild type and GFAPTrkB KO mice at any time point, indicating that astrocyte TrkB does not rule glutamate transporter levels *in vivo* after stroke.

3.4. Astrocyte TrkB sustains edema and AQP4 levels in experimental ischemic stroke

Cerebral edema is an acute complication of ischemic stroke, and when severe is associated with poor prognosis (Battey et al., 2014; McKeown et al., 2022). To evaluate the effect of astrocyte TrkB on the development of cerebral edema we measured the enlargement of the ischemic hemispheres compared to the contralateral areas in GFAPTrkB KO and WT animals at day 1 p.i. (Fig. 4A). We observed that GFAPTrkB KO animals had limited ischemic swelling compared to control TrkB WT mice (Fig. 4A-B). Cerebral swelling after ischemia is generated by an

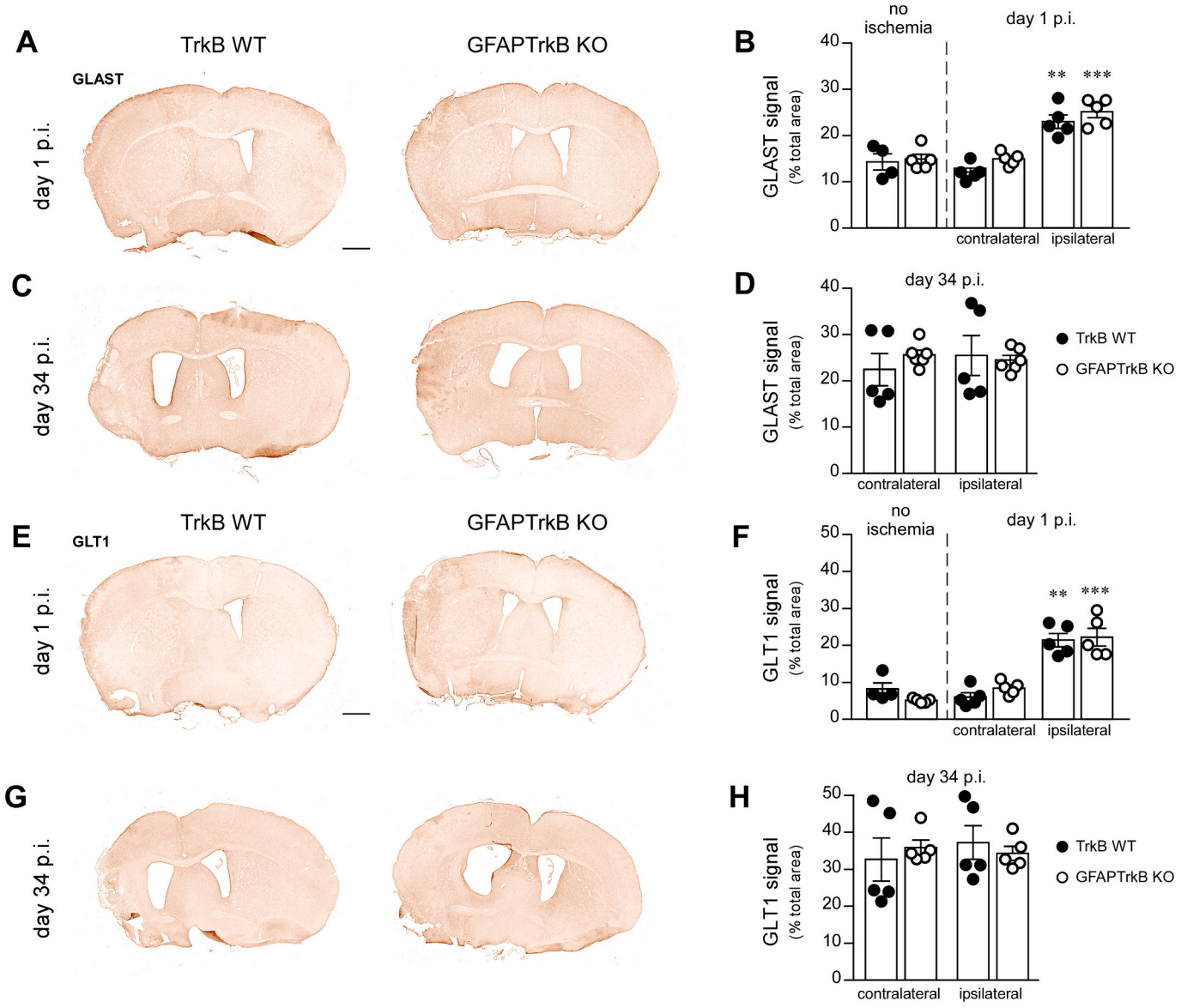

Fig. 3. Astrocyte TrkB does not support glutamate transporter expression. (A-D) Representative brain immunohistochemistry for GLAST in TrkB WT and GFAPTrkB KO mice at day 1 (A) or 34 (C) p.i.. and signal quantification (B, D) in the contralateral and ipsilateral hemispheres of non-ischemic animals and mice subjected to MCAO. (E-H) The same as in (A-D) for GLT1 stains. Asterisks indicate statistical significance *versus* no ischemia. ***P < 0.001, **P < 0.01. In B, D, F, H, each dot represents a single animal; bars represent means of the values ± SEM. Scale bars 800 μm.

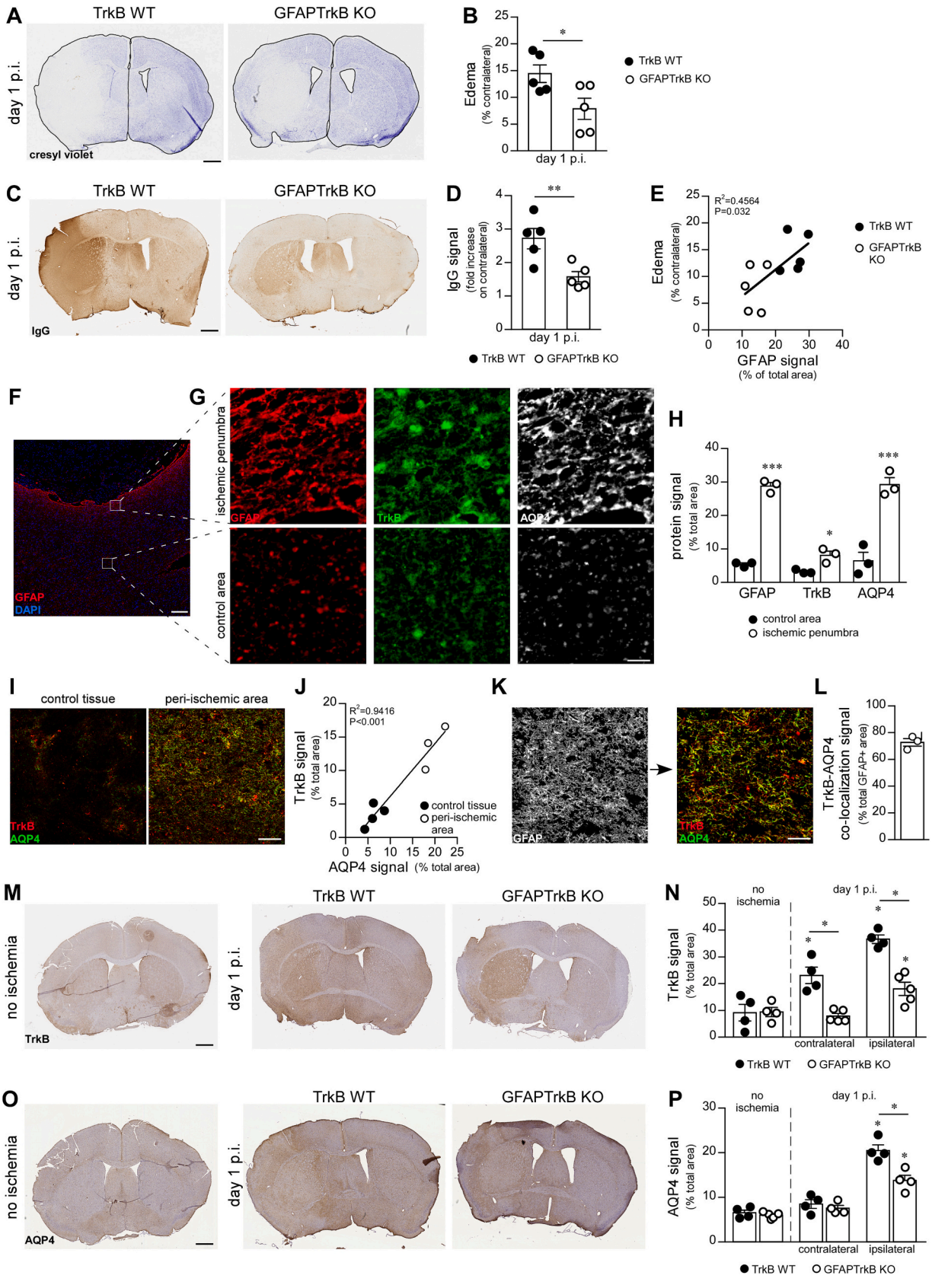

(caption on next page)

Fig. 4. Astrocyte TrkB deletion controls edema exacerbation in experimental ischemic stroke. (A-B) Representative ischemic brain sections of TrkB WT and GFAPTrkB KO mice stained with cresyl violet at day 1 p.i. (A) and relative edema quantifications (B). Black lines outline ipsilateral and contralateral hemispheres. (C—D) Representative brain immunohistochemistry for IgG in TrkB WT and GFAPTrkB KO mice at day 1 p.i. (C) and relative quantifications (D). (E) Correlation between edema and GFAP expression in the ischemic hemisphere of TrkB WT and GFAPTrkB KO mice. (F) Representative immunofluorescence stain for GFAP in human acute ischemic tissue. (G-H) Stains for GFAP (left panels), TrkB (middle panels) and AQP4 (right panels) in ischemic penumbra (upper panels) and control areas (lower panels) (G) and signal quantification (n = 3) (H). (I) Representative confocal imaging for TrkB (red) and AQP4 (green) in control (left panel) or peri-ischemic (right panel) brain tissue. (J) Correlation between TrkB and AQP4 expression in control (n = 4) and peri-ischemic tissues (n = 3). (K-L) Analysis of TrkB-AQP4 co-localization in GFAP positive cells. Regions of interests (ROIs) were generated on GFAP images (K), ROIs were applied to the corresponding TrkB and AQP4 images, and co-localization signals were counted (L). (M-N) Representative brain TrkB immunohistochemistry in non-ischemic mice (M, left panel) or ischemic TrkB WT or GFAPTrkB KO animals at day 1 p.i. (M, middle and right panels) and relative quantification (N). (O—P) The same as in (M-N) for AQP4 stains. Asterisks indicate statistical significance *versus* no ischemia. Asterisks above bar indicate statistical significance between different genotypes/control area. $^{**}P < 0.01$, $^{*}P < 0.05$. In B, D, E, H, J, L, N, P each dot represents a single sample/animal; bars represent means of the values ± SEM. Scale bars 800 μm in A, C, M, O; 200 μm in F; 50 μm in I—K, and 20 μm in G. (For interpretation of the references to colour in this figure legend, the reader is referred to the web version of this article.)

inflow of fluids composed of water, ions and, eventually, proteins such as IgG, into CNS parenchyma and is partly contributed by blood brain barrier (BBB) leakage (Okada et al., 2020). IgG labeling in ischemic mice showed that IgG levels were almost halved in GFAPTrkB KO animals compared to controls (Fig. 4C-D), indicating a role for astrocyte TrkB to BBB breakdown after stroke.

Astrocytes are a main constituent of the BBB and their endfeet, which encase the vasculature, express AQP4, a key protein channel for water homeostasis (Rasmussen et al., 2022). As edema levels significantly correlated with astrogliosis (Fig. 4E), we verified AQP4 and TrkB levels and their colocalization in human tissues. A few hours after ischemic stroke, human GFAP protein was significantly augmented in ischemic penumbra in comparison to adjacent control areas (Fig. 4F-H). Importantly, gliosis was accompanied by significant upregulation of TrkB and AQP4 in acute ischemic stroke samples (Fig. 4G-H). Similarly, human chronic peri-ischemic areas were characterized by concomitant upregulation of TrkB and AQP4, whose levels correlated positively (Fig. 4I-J). Notably, co-localization analyses of GFAP, TrkB and AQP4 proteins revealed that about 73 % of GFAP positive area also showed signals for TrkB and AQP4 in peri-infarct regions (Fig. 4K-L). When analyzing brain sections from control or ischemic TrkB WT or GFAPTrkB KO mice, TrkB signals were low in healthy CNS and enhanced in ischemic tissues, though at significantly lower levels in GFAPTrkB KO mice compared to TrkB WT animals (Fig. 4M-N). Similarly, AQP4 signal greatly augmented at day 1 p.i. in all animals compared to non-ischemic animals (Fig. 4O left and middle panels and Fig. 4P). Notably, AQP4 protein levels were 30 % lower in ischemic GFAPTrkB KO mice than in control littermates (Fig. 4O right panel and Fig. 4P), demonstrating early and robust astrocyte TrkB-dependent regulation of AQP4 after ischemic stroke.

3.5. Astrocyte TrkB supports AQP4 levels under hypoxia

As our *in vivo* data indicated that astrocyte TrkB may support rapid AQP4 induction in ischemic brain, we searched for a direct functional link between TrkB signaling and AQP4 expression in astrocytes. We cultured primary mouse astrocytes for 24 h under oxygen deprivation to mimic *in vivo* hypoxic conditions and initially checked the expression and localization of the transcription factor HIF-1α to validate our *in vitro* hypoxia model. While present in perinuclear areas under normoxic conditions, HIF-1α stain became localized in the nuclei under hypoxia (Fig. 5A-B). To check the impact of TrkB signaling on HIF-1α activation *in vitro,* we compared the nuclear translocation of HIF-1α in TrkB WT and KO astrocytes under hypoxia. As shown in Fig. 5 C—D, HIF-1α positive nuclei were more frequent in control than TrkB KO astrocytes after 6 h oxygen deprivation, while no difference was observed at a later time point (Fig. 5E), indicating that TrkB signaling supports early activation of the transcription factor.

We then analyzed TrkB protein levels and noticed that *in vitro* hypoxia significantly increased TrkB levels in astrocytes after 24 h (Supplementary Fig. 1, and Fig. 5F-G), indicating that oxygen deprivation may directly modulate glial TrkB expression. Similarly, hypoxia enhanced AQP4 expression (Fig. 5H, J). Notably, AQP4 protein levels remained low in TrkB KO astrocytes exposed to oxygen deprivation (Fig. 5I, J white dots), demonstrating that TrkB signaling directly operates downstream hypoxic signals to support AQP4 upregulation in glia cells.

To verify whether activation of HIF-1α was necessary for TrkB and AQP4 upregulation under hypoxia, we exposed WT astrocytes to 2ME2, a natural compound with HIF-1α inhibitory activity (Ma et al., 2014), or vehicle for 2 h under normoxic conditions, then changed the medium and incubated the cells under normoxia or hypoxia for further 24 h. As control, immunofluorescence for HIF-1α confirmed lower nuclear signal in 2ME2-treated cells compared with non-treated astrocytes after oxygen deprivation (Supplementary Fig. 2). Importantly, TrkB protein levels were up-regulated in astrocytes under hypoxia even when cells were pre-exposed to 2ME2 (Fig. 5K, M black dots), while hypoxia-induced AQP4 expression was completely prevented by 2ME2 treatment (Fig. 5L-M white dots). Overall, these *in vitro* experiments demonstrate that HIF-1α activation does not control TrkB levels but is necessary for AQP4 regulation in astrocytes under hypoxia.

4. Discussion

In this study we report that following cerebral ischemia astrocytes upregulate the neurotrophin receptor TrkB, thereby increasing CNS tissue damage and promoting cerebral edema *via* increasing AQP4 levels.

While occasionally expressed on astrocytes in adult CNS under physiological conditions, TrkB may be induced under neuroinflammatory conditions, such as multiple sclerosis and its animal models (Colombo et al., 2012; Colombo et al., 2021). Here we showed that this event may take place also at acute and chronic phases of post-ischemic damage. In harmony with these *ex vivo* observations, our *in vivo* stroke studies with GFAPTrkB KO and control mice demonstrate that astrocyte TrkB deletion reduces astrogliosis in the infarcted hemisphere. TrkB regulates astrocyte maturation during development (Holt et al., 2019) and is downregulated postnatally, so that its levels in astrocytes are low/absent in adult CNS under physiological conditions (Colombo et al., 2021; Colombo et al., 2012). Tissue injury may lead to novel TrkB expression in astrocytes, where it supports astrocyte proliferation and scar formation as shown during neuroinflammation (Matyas et al., 2017; Colombo et al., 2021) or after stroke (this paper).

Notably, TrkB-dependent astrocyte activation sustains neurological dysfunction measured as limb paralysis in the experimental model of multiple sclerosis (Colombo et al., 2012) and as decreased motor coordination in the stroke model utilized in this study, which suggests that interference with a single signaling pathway in a specific cell type may support clinical amelioration. Our neuropathological studies show reduced lesion area, BBB breakdown and edema in GFAPTrkB KO mice already at 24 h p.i., which results in limited ischemic volume and brain atrophy in the chronic phase after ischemia. These evidences point to an early involvement of TrkB signaling in astrocyte activation favoring the development of ischemic pathology, however further studies are necessary to understand whether interventions targeting astrocyte TrkB

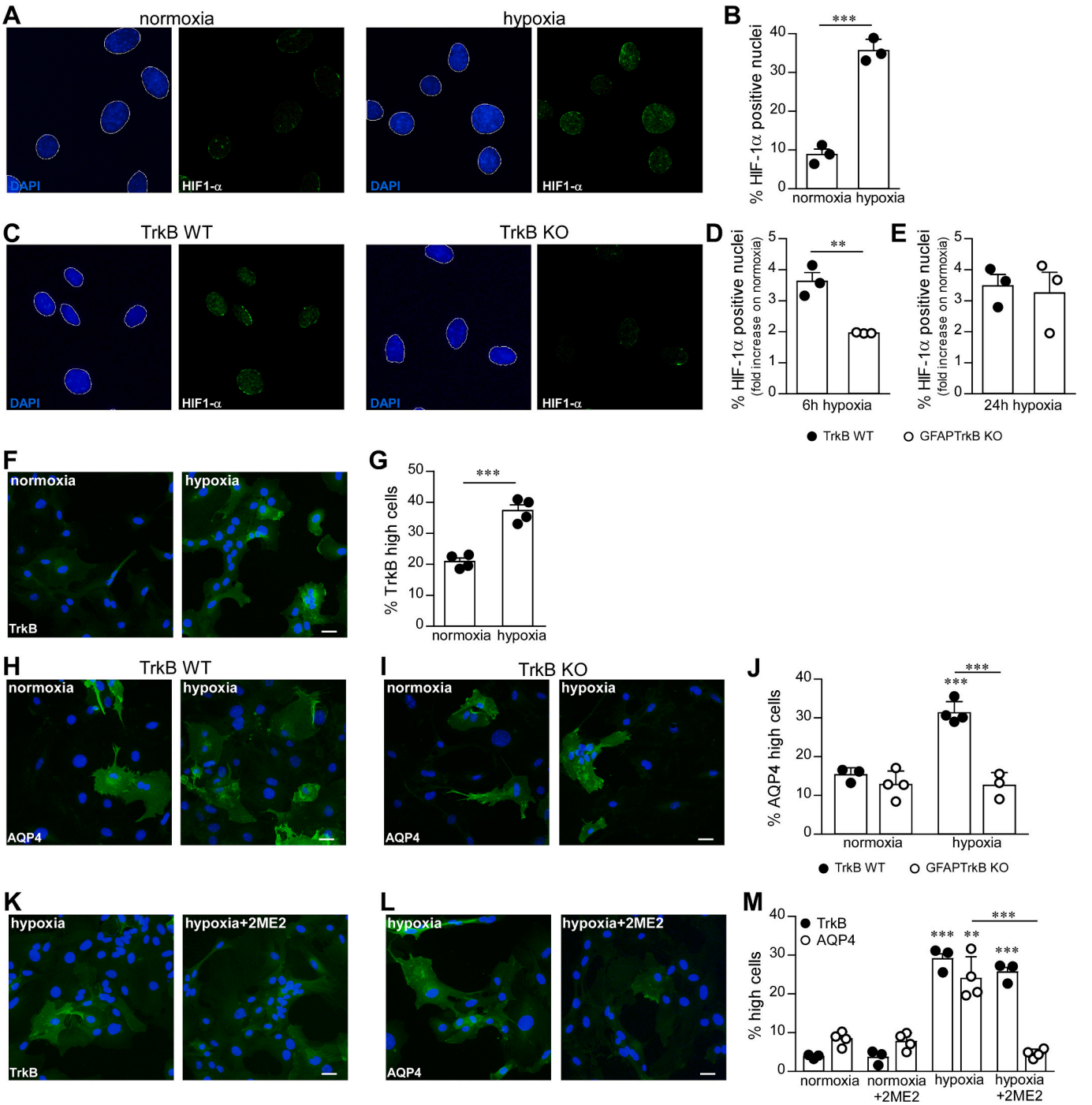

Fig. 5. AQP4 up-regulation in astrocytes is dependent on TrkB. (A-B) Representative immunofluorescence stains (A) and quantification (B) of nuclear HIF-1α signal in primary TrkB WT astrocytes under normoxia or 24 h hypoxia. (C) Representative images for HIF-1α in TrkB WT and GFAPTrkB KO astrocytes after 6 h hypoxia. (D-E) Quantification of HIF-1α positive nuclei in astrocytes after 6 h (D) or 24 h (E) hypoxia expressed as fold change relative to normoxia. (F-G) TrkB signal in TrkBWT astrocytes under normoxia or hypoxia for 24 h (F) and quantification of TrkB high cells (G). (H—I) Immunofluorescence for AQP4 in TrkB WT (H) and GFAPTrkB KO (I) astrocytes under 24 h normoxia or hypoxia. (J) Quantification of AQP4 levels at distinct culture conditions. (K-M) Representative immunofluorescence stains for TrkB (K) and AQP4 (L) in TrkB WT astrocytes under normoxia or hypoxia eventually after pre-treatment with 2ME2, and (M) relative quantifications. Asterisks indicate statistical significance *versus* normal conditions from the same genotype. Asterisks above the bar indicate statistical significance between genotypes or specific conditions. ***P < 0.001, **P < 0.01, *P < 0.05. In B, G, J, M representative data of one out of three independent experiments is reported as means of the values ± SD and each dot represents a technical replicate. In D and E the sum of three independent experiments is reported as means of the values ± SEM and each dot represents a different cell preparations. Scale bars 30 μm.

after injury may also hinder ongoing detrimental processes.

Glutamate accumulation in the brain occurs quickly after stroke (Hurtado et al., 2003; Mitani and Tanaka, 2003), can lead to neuronal cell death through a process defined as glutamate excitotoxicity (Verma et al., 2022) and can be regulated by the transporters GLAST and GLT1 expressed on astrocytes (Kaplan-Arabaci et al., 2022). Some studies report up-regulation of glutamate transporters in astrocytes after transient ischemia (Arranz et al., 2010; Bacigaluppi et al., 2016), which may

suggest the activation of a tissue protective mechanism attenuating local excitotoxicity. Our histological data revealed augmented protein levels of GLAST and GLT1, initially limited to the ischemic hemisphere and later throughout the brain, which were independent of mouse genotypes, indicating that astrocyte TrkB does not regulate glutamate transporter levels *in vivo* after stroke.

Cerebral ischemia or *in vitro* hypoxia may increase AQP4 levels on astrocytes (our data, (Zeng et al., 2010, Kitchen et al., 2020)). The rise in cellular water uptake *via* AQP4 during the early phase of cerebral ischemia promotes edema and impacts on stroke morbidity as it augments intracranial pressure, reduces cerebral blood flow and fosters neuronal death (Patabendige and Chen, 2022). Transgenic mice deficient for AQP4 are relatively protected from brain edema and damage after cerebral ischemia, indicating that AQP4 is a crucial regulator of edema (Manley et al., 2000; Yao et al., 2015; Hirt et al., 2017). Here we demonstrated that AQP4 upregulation after damage may depend on TrkB signaling, as TrkB deletion in astrocytes is sufficient to impair adaptive AQP4 levels in response to cerebral ischemia and hypoxia.

Several signals may activate TrkB signaling. Regarding TrkB ligands, intraventricular or intravenous administration of BDNF is protective in stroke as it reduces infarct size and neuronal loss (Schabitz et al., 2000; Zhang and Pardridge, 2006). Similarly, intracerebral transplantation of BDNF-overexpressing cells promotes functional recovery (Kurozumi et al., 2004; Chen et al., 2012). However, TrkB requirement for BDNF action under these conditions is not proven, leaving open the possibility that neurotrophins mediate protection *via* other receptors. On the other hand, TrkB can be transactivated independently of neurotrophin binding, as shown for GPCR-signaling (Lee and Chao, 2001), inflammatory and toxic signaling (Colombo et al., 2021). TrkB transactivation rules key steps in astrocyte activation such as calcium flux and cell proliferation (Colombo et al., 2021). Importantly, intracellular calcium flux and NF-κB activation are implicated in AQP4 upregulation (Ito et al., 2006; Kitchen et al., 2020; Lu et al., 2022; Stokum et al., 2023). Further, calcium signaling stimulates translation of HIF-1α during hypoxia (Hui et al., 2006) and NFkB may enhance HIF-1α mRNA transcription and protein stabilization (Tacchini et al., 2004; Bonello et al., 2007; van Uden et al., 2008; Jin et al., 2018). Here we describe that the intermediate step of the TrkB pathway regulating AQP4 levels is the activation of the transcription factor HIF-1α, which may translocate to the nucleus under hypoxic conditions and activate gene transcription at specific hypoxia responsive elements (Mitroshina et al., 2021). Administration of the HIF-1α inhibitor 2ME2 after traumatic brain injury restrains AQP4 levels (Ding et al., 2009; Higashida et al., 2011; Xiong et al., 2022) and reduces brain water content (Higashida et al., 2011, Xiong et al., 2022), BBB breakdown and neurological deficits (Xiong et al., 2022). Importantly, HIF-1α inhibitors protect animals from ischemic damage only if provided immediately after stroke (Yeh et al., 2007; Yeh et al., 2011; Na et al., 2015), indicating that early activation of HIF-1α in the acute phase of ischemic stroke represents a detrimental tissue response to damage. Here we described a link between TrkB signaling and HIF-1α activation, as deletion of TrkB slows nuclear translocation of HIF-1α in astrocytes under oxygen deprivation, and between HIF-1α activation and AQP4 levels, as HIF-1α inhibition is sufficient to prevent AQP4 upregulation under hypoxia, but additional studies are necessary to finely describe all intermediate signaling steps.

In summary our data indicate that astrocyte TrkB drives neurological impairment, lesion development and brain edema after stroke and that it may regulate AQP4 levels *via* HIF-1α activation.

Funding

This work was funded by the Italian Ministry for Health (Ricerca Corrente).

Ethics approval and consent to participate

All procedures involving animals were authorized by the local Animal Ethical Committee and the Italian General Direction for Animal Health at the Ministry of Health.

Tissues from subjects with acute ischemia were obtained at autopsy according to the Review Board-approved protocol at Department of Neurology, Yale School of Medicine, USA. Chronic cerebral infarct and control samples were provided by the NeuroResource tissue bank (UCL Queen Square Institute of Neurology, London, UK) and donated with informed consent using documentation approved by the NHS NRES Ethics Committee London–Central, UK.

CRediT authorship contribution statement

Emanuela Colombo: Writing – review & editing, Writing – original draft, Methodology, Investigation, Formal analysis, Data curation. **Michela Bartoccetti:** Methodology, Formal analysis. **Daniela Triolo:** Methodology, Formal analysis. **Claudia Bassani:** Methodology, Formal analysis. **Andrea Bergamaschi:** Methodology. Hélène C. Descamps: Methodology. **Giorgia Serena Gullotta:** Methodology, Formal analysis. **Maria Henley:** Resources, Methodology. **Marco Piccoli:** Resources, Methodology. **Luigi Anastasia:** Resources. **David Pitt:** Resources, Methodology. **Jia Newcombe:** Resources. **Gianvito Martino:** Resources, Methodology. **Cinthia Farina:** Writing – review & editing, Writing – original draft, Validation, Supervision, Resources, Project administration, Methodology, Funding acquisition, Formal analysis, Conceptualization.

Declaration of competing interest

The authors declare that they have no known competing financial interests or personal relationships that could have appeared to influence the work reported in this paper.

Data availability

Data generated or analyzed during this study are included in this published article (and its supplementary information files).

Appendix A. Supplementary data

Supplementary data to this article can be found online at https://doi.org/10.1016/j.nbd.2024.106670.

References

Arranz, A.M., Gottlieb, M., Perez-Cerda, F., Matute, C., 2010. Increased expression of glutamate transporters in subcortical white matter after transient focal cerebral ischemia. Neurobiol. Dis. 37, 156–165.

Bacigaluppi, M., Russo, G.L., Peruzzotti-Jametti, L., Rossi, S., Sandrone, S., Butti, E., De Ceglia, R., Bergamaschi, A., Motta, C., Gallizioli, M., Studer, V., Colombo, E., Farina, C., Comi, G., Politi, L.S., Muzio, L., Villani, C., Invernizzi, R.W., Hermann, D. M., Centonze, D., Martino, G., 2016. Neural stem cell transplantation induces stroke recovery by upregulating glutamate transporter GLT-1 in astrocytes. J. Neurosci. 36, 10529–10544.

Balkaya, M., Krober, J.M., Rex, A., Endres, M., 2013. Assessing post-stroke behavior in mouse models of focal ischemia. J. Cereb. Blood Flow Metab. 33, 330–338.

Battey, T.W.K., Karki, M., Singhal, A.B., Wu, O., Sadaghiani, S., Campbell, B.C.V., Davis, S.M., Donnan, G.A., Sheth, K.N., Kimberly, W.T., 2014. Brain edema predicts outcome after nonlacunar ischemic stroke. Stroke 45, 3643–3648.

Bonello, S., Zahringer, C., BelAiba, R.S., Djordjevic, T., Hess, J., Michiels, C., Kietzmann, T., Gorlach, A., 2007. Reactive oxygen species activate the HIF-1alpha promoter via a functional NFkappaB site. Arterioscler. Thromb. Vasc. Biol. 27, 755–761.

Campbell, B.C.V., Khatri, P., 2020. Stroke. Lancet 396, 129–142.

Cekanaviciute, E., Fathali, N., Doyle, K.P., Williams, A.M., Han, J., Buckwalter, M.S., 2014. Astrocytic transforming growth factor-beta signaling reduces subacute neuroinflammation after stroke in mice. Glia 62, 1227–1240.

Chamorro, A., Lo, E.H., Renu, A., van Leyen, K., Lyden, P.D., 2021. The future of neuroprotection in stroke. J. Neurol. Neurosurg. Psychiatry 92, 129–135.

Chen, S., Tsai, J., Lin, T., Chang, C., Tseng, T., Chien, C., 2012. Brain-derived neurotrophic factor-transfected and nontransfected 3T3 fibroblasts enhance migratory neuroblasts and functional restoration in mice with intracerebral hemorrhage. J. Neuropathol. Exp. Neurol. 71, 1123–1136.
Colombo, E., Farina, C., 2016. Astrocytes: key regulators of Neuroinflammation. Trends Immunol. 37, 608–620.
Colombo, E., Cordiglieri, C., Melli, G., Newcombe, J., Krumbholz, M., Parada, L.F., Medico, E., Hohlfeld, R., Meinl, E., Farina, C., 2012. Stimulation of the neurotrophin receptor TrkB on astrocytes drives nitric oxide production and neurodegeneration. J. Exp. Med. 209, 521–535.
Colombo, E., Triolo, D., Bassani, C., Bedogni, F., Di Dario, M., Dina, G., Fredrickx, E., Fermo, I., Martinelli, V., Newcombe, J., Taveggia, C., Quattrini, A., Comi, G., Farina, C., 2021. Dysregulated copper transport in multiple sclerosis may cause demyelination via astrocytes. Proc. Natl. Acad. Sci. USA 118. https://doi.org/10.1073/pnas.2025804118.
Ding, J.Y., Kreipke, C.W., Speirs, S.L., Schafer, P., Schafer, S., Rafols, J.A., 2009. Hypoxia-inducible factor-1alpha signaling in aquaporin upregulation after traumatic brain injury. Neurosci. Lett. 453, 68–72.
Dvoriantchikova, G., Barakat, D., Brambilla, R., Agudelo, C., Hernandez, E., Bethea, J.R., Shestopalov, V.I., Ivanov, D., 2009. Inactivation of astroglial NF-kappa B promotes survival of retinal neurons following ischemic injury. Eur. J. Neurosci. 30, 175–185.
Gullotta, G.S., De Feo, D., Friebel, E., Semerano, A., Scotti, G.M., Bergamaschi, A., Butti, E., Brambilla, E., Genchi, A., Capotondo, A., Gallizioli, M., Coviello, S., Piccoli, M., Vigo, T., Della Valle, P., Ronchi, P., Comi, G., D'Angelo, A., Maugeri, N., Roveri, L., Uccelli, A., Becher, B., Martino, G., Bacigaluppi, M., 2023. Age-induced alterations of granulopoiesis generate atypical neutrophils that aggravate stroke pathology. Nat. Immunol. 24, 925–940.
Higashida, T., Kreipke, C.W., Rafols, J.A., Peng, C., Schafer, S., Schafer, P., Ding, J.Y., Dornbos, D., Li, X., Guthikonda, M., Rossi, N.F., Ding, Y., 2011. The role of hypoxia-inducible factor-1alpha, aquaporin-4, and matrix metalloproteinase-9 in blood-brain barrier disruption and brain edema after traumatic brain injury. J. Neurosurg. 114, 92–101.
Hirt, L., Fukuda, A.M., Ambadipudi, K., Rashid, F., Binder, D., Verkman, A., Ashwal, S., Obenaus, A., Badaut, J., 2017. Improved long-term outcome after transient cerebral ischemia in aquaporin-4 knockout mice. J. Cereb. Blood Flow Metab. 37, 277–290.
Holt, L.M., Hernandez, R.D., Pacheco, N.L., Torres Ceja, B., Hossain, M., Olsen, M.L., 2019. Astrocyte morphogenesis is dependent on BDNF signaling via astrocytic TrkB.T1. Elife 8. https://doi.org/10.7554/eLife.44667.
Hui, A.S., Bauer, A.L., Striet, J.B., Schnell, P.O., Czyzyk-Krzeska, M.F., 2006. Calcium signaling stimulates translation of HIF-alpha during hypoxia. FASEB J. 20, 466–475.
Hurtado, O., De Cristobal, J., Sanchez, V., Lizasoain, I., Cardenas, A., Pereira, M.P., Colado, M.I., Leza, J.C., Lorenzo, P., Moro, M.A., 2003. Inhibition of glutamate release by delaying ATP fall accounts for neuroprotective effects of antioxidants in experimental stroke. FASEB J. 17, 2082–2084.
Ito, H., Yamamoto, N., Arima, H., Hirate, H., Morishima, T., Umenishi, F., Tada, T., Asai, K., Katsuya, H., Sobue, K., 2006. Interleukin-1beta induces the expression of aquaporin-4 through a nuclear factor-kappaB pathway in rat astrocytes. J. Neurochem. 99, 107–118.
Jin, P., Shin, S., Chun, Y., Shin, H., Shin, Y.J., Lee, Y., Kim, D., Nam, D., Park, J., 2018. Astrocyte-derived CCL20 reinforces HIF-1-mediated hypoxic responses in glioblastoma by stimulating the CCR6-NF-kappaB signaling pathway. Oncogene 37, 3070–3087.
Kaplan-Arabaci, O., Acari, A., Ciftci, P., Gozuacik, D., 2022. Glutamate scavenging as a Neuroreparative strategy in ischemic stroke. Front. Pharmacol. 13, 866738.
Kitchen, P., Salman, M.M., Halsey, A.M., Clarke-Bland, C., MacDonald, J.A., Ishida, H., Vogel, H.J., Almutiri, S., Logan, A., Kreida, S., Al-Jubair, T., Winkel Missel, J., Gourdon, P., Tornroth-Horsefield, S., Conner, M.T., Ahmed, Z., Conner, A.C., Bill, R. M., 2020. Targeting Aquaporin-4 subcellular localization to treat central nervous system edema. Cell 181, 784–799.e19.
Kurozumi, K., Nakamura, K., Tamiya, T., Kawano, Y., Kobune, M., Hirai, S., Uchida, H., Sasaki, K., Ito, Y., Kato, K., Honmou, O., Houkin, K., Date, I., Hamada, H., 2004. BDNF gene-modified mesenchymal stem cells promote functional recovery and reduce infarct size in the rat middle cerebral artery occlusion model. Mol. Ther. 9, 189–197.
Lee, F.S., Chao, M.V., 2001. Activation of Trk neurotrophin receptors in the absence of neurotrophins. Proc. Natl. Acad. Sci. USA 98, 3555–3560.
Li, L., Lundkvist, A., Andersson, D., Wilhelmsson, U., Nagai, N., Pardo, A.C., Nodin, C., Stahlberg, A., Aprico, K., Larsson, K., Yabe, T., Moons, L., Fotheringham, A., Davies, I., Carmeliet, P., Schwartz, J.P., Pekna, M., Kubista, M., Blomstrand, F., Maragakis, N., Nilsson, M., Pekny, M., 2008. Protective role of reactive astrocytes in brain ischemia. J. Cereb. Blood Flow Metab. 28, 468–481.
Lin, T.N., He, Y.Y., Wu, G., Khan, M., Hsu, C.Y., 1993. Effect of brain edema on infarct volume in a focal cerebral ischemia model in rats. Stroke 24, 117–121.
Lo, A.C.Y., Chen, A.Y.S., Hung, V.K.L., Yaw, L.P., Fung, M.K.L., Ho, M.C.Y., Tsang, M.C. S., Chung, S.S.M., Chung, S.K., 2005. Endothelin-1 overexpression leads to further water accumulation and brain edema after middle cerebral artery occlusion via aquaporin 4 expression in astrocytic end-feet. J. Cereb. Blood Flow Metab. 25, 998–1011.
Lu, H., Ai, L., Zhang, B., 2022. TNF-alpha induces AQP4 overexpression in astrocytes through the NF-kappaB pathway causing cellular edema and apoptosis. Biosci. Rep. 42, BSR20212224. https://doi.org/10.1042/BSR20212224.
Ma, L., Li, G., Zhu, H., Dong, X., Zhao, D., Jiang, X., Li, J., Qiao, H., Ni, S., Sun, X., 2014. 2-Methoxyestradiol synergizes with sorafenib to suppress hepatocellular carcinoma by simultaneously dysregulating hypoxia-inducible factor-1 and -2. Cancer Lett. 355, 96–105.
Ma, R., Xie, Q., Li, Y., Chen, Z., Ren, M., Chen, H., Li, H., Li, J., Wang, J., 2020. Animal models of cerebral ischemia: a review. Biomed. Pharmacother. 131, 110686.
Manley, G.T., Fujimura, M., Ma, T., Noshita, N., Filiz, F., Bollen, A.W., Chan, P., Verkman, A.S., 2000. Aquaporin-4 deletion in mice reduces brain edema after acute water intoxication and ischemic stroke. Nat. Med. 6, 159–163.
Matyas, J.J., O'Driscoll, C.M., Yu, L., Coll-Miro, M., Daugherty, S., Renn, C.L., Faden, A. I., Dorsey, S.G., Wu, J., 2017. Truncated TrkB.T1-mediated astrocyte dysfunction contributes to impaired motor function and neuropathic pain after spinal cord injury. J. Neurosci. 37, 3956–3971.
McKeown, M.E., Prasad, A., Kobsa, J., Top, I., Snider, S.B., Kidwell, C., Campbell, B.C.V., Davis, S.M., Donnan, G.A., Lev, M., Sheth, K.N., Petersen, N., Kimberly, W.T., Bevers, M.B., 2022. Midline shift greater than 3 mm independently predicts outcome after ischemic stroke. Neurocrit. Care. 36, 46–51.
Mitani, A., Tanaka, K., 2003. Functional changes of glial glutamate transporter GLT-1 during ischemia: an in vivo study in the hippocampal CA1 of normal mice and mutant mice lacking GLT-1. J. Neurosci. 23, 7176–7182.
Mitroshina, E.V., Savyuk, M.O., Ponimaskin, E., Vedunova, M.V., 2021. Hypoxia-inducible factor (HIF) in ischemic stroke and neurodegenerative disease. Front. Cell Dev. Biol. 9, 703084.
Na, J., Na, J., Choi, W., Lee, M., Park, M., Choi, K., Lee, J., Kim, K., Park, J., Kim, H., 2015. The HIF-1 inhibitor YC-1 decreases reactive astrocyte formation in a rodent ischemia model. Am. J. Transl. Res. 7, 751–760.
Okada, T., Suzuki, H., Travis, Z.D., Zhang, J.H., 2020. The stroke-induced blood-brain barrier disruption: current Progress of inspection technique, mechanism, and therapeutic target. Curr. Neuropharmacol. 18, 1187–1212.
Overman, J.J., Clarkson, A.N., Wanner, I.B., Overman, W.T., Eckstein, I., Maguire, J.L., Dinov, I.D., Toga, A.W., Carmichael, S.T., 2012. A role for ephrin-A5 in axonal sprouting, recovery, and activity-dependent plasticity after stroke. Proc. Natl. Acad. Sci. USA 109, 2230.
Patabendige, A., Chen, R., 2022. Astrocytic aquaporin 4 subcellular translocation as a therapeutic target for cytotoxic edema in ischemic stroke. Neural Regen. Res. 17, 2666–2668.
Rasmussen, M.K., Mestre, H., Nedergaard, M., 2022. Fluid transport in the brain. Physiol. Rev. 102, 1025–1151.
Schabitz, W.R., Sommer, C., Zoder, W., Kiessling, M., Schwaninger, M., Schwab, S., 2000. Intravenous brain-derived neurotrophic factor reduces infarct size and counterregulates Bax and Bcl-2 expression after temporary focal cerebral ischemia. Stroke 31, 2212–2217.
Shen, X., Gao, Z., Han, Y., Yuan, M., Guo, Y., Bi, X., 2021. Activation and role of astrocytes in ischemic stroke. Front. Cell. Neurosci. 15, 755955.
Stokum, J.A., Shim, B., Negoita, S., Tsymbalyuk, N., Tsymbalyuk, O., Ivanova, S., Keledjian, K., Bryan, J., Blaustein, M.P., Jha, R.M., Kahle, K.T., Gerzanich, V., Simard, J.M., 2023. Cation flux through SUR1-TRPM4 and NCX1 in astrocyte endfeet induces water influx through AQP4 and brain swelling after ischemic stroke. Sci. Signal. 16, eadd6364.
Tacchini, L., De Ponti, C., Matteucci, E., Follis, R., Desiderio, M.A., 2004. Hepatocyte growth factor-activated NF-kappaB regulates HIF-1 activity and ODC expression, implicated in survival, differently in different carcinoma cell lines. Carcinogenesis 25, 2089–2100.
van Uden, P., Kenneth, N.S., Rocha, S., 2008. Regulation of hypoxia-inducible factor-1alpha by NF-kappaB. Biochem. J. 412, 477–484.
Verma, M., Lizama, B.N., Chu, C.T., 2022. Excitotoxicity, calcium and mitochondria: a triad in synaptic neurodegeneration. Transl. Neurodegen. 11, 3–7.
Xiong, A., Li, J., Xiong, R., Xia, Y., Jiang, X., Cao, F., Lu, H., Xu, J., Shan, F., 2022. Inhibition of HIF-1alpha-AQP4 axis ameliorates brain edema and neurological functional deficits in a rat controlled cortical injury (CCI) model. Sci. Rep. 12, 2701–2709.
Yang, S., Liu, R., 2021. Four decades of ischemic penumbra and its implication for ischemic stroke. Transl. Stroke Res. 12, 937–945.
Yao, X., Derugin, N., Manley, G.T., Verkman, A.S., 2015. Reduced brain edema and infarct volume in aquaporin-4 deficient mice after transient focal cerebral ischemia. Neurosci. Lett. 584, 368–372.
Yeh, S., Ou, L., Gean, P., Hung, J., Chang, W., 2011. Selective inhibition of early–but not late–expressed HIF-1alpha is neuroprotective in rats after focal ischemic brain damage. Brain Pathol. 21, 249–262.
Yeh, W., Lu, D., Lin, C., Liou, H., Fu, W., 2007. Inhibition of hypoxia-induced increase of blood-brain barrier permeability by YC-1 through the antagonism of HIF-1alpha accumulation and VEGF expression. Mol. Pharmacol. 72, 440–449.
Zeng, H.K., Wang, Q.S., Deng, Y.Y., Fang, M., Chen, C.B., Fu, Y.H., Jiang, W.Q., Jiang, X., 2010. Hypertonic saline ameliorates cerebral edema through downregulation of aquaporin-4 expression in the astrocytes. Neuroscience 166, 878–885.
Zhang, Y., Pardridge, W.M., 2006. Blood-brain barrier targeting of BDNF improves motor function in rats with middle cerebral artery occlusion. Brain Res. 1111, 227–229.